

# Indonesian Journal of Computing, Engineering, and Design

Journal homepage: <a href="http://ojs.sampoernauniversity.ac.id/index.php/IJOCED">http://ojs.sampoernauniversity.ac.id/index.php/IJOCED</a>

# Effect of Chip Breaker Geometries on Cutting Force: A Finite Element Analysis

Mohd Fawzi Zamria<sup>1</sup>, Mohd Nor Sufyan Sudin<sup>1</sup>, Cucuk Nur Rosyidi<sup>2</sup>, Ahmad Razlan Yusoff<sup>1,3\*</sup>

<sup>1</sup> Faculty of Manufacturing and Mechatronic Engineering Technology Universiti Malaysia Pahang Al-Sultan Abdullah, 26600 Pekan, Pahang, Malaysia

<sup>2</sup>Industrial Engineering Department, Faculty of Engineering, Universitas Sebelas Maret, Surakarta, Indonesia <sup>3</sup> Centre for Advanced Industrial Technology, Universiti Malaysia Pahang Al-Sultan Abdullah, 26600 Pekan, Pahang, Malaysia

Corresponding email: razlan@umpsa.edu.my

## ABSTRACT

Continuous chip formation during metal cutting operations poses substantial challenges, from deteriorating surface finish to accelerated tool wear. Our research examines how six chip breaker geometric parameters of insert rake angle, land, radius, width, height, and nose radius influence cutting forces in turning operations. Using DEFORM-3D, we simulated 27 distinct chip breaker configurations based on Taguchi's L27 orthogonal array while maintaining constant cutting parameters of 275 mm/min speed, 0.2 mm/rev feed, and 1.0 mm depth. ANOVA findings showed that nose radius was most influential with F-ratio equal to 27.41, followed by insert width and rake angle. The optimized geometry of the rake angle is 16°, the land is 0.1 mm, the radius is 0.5 mm, width is 2.0 mm, height is 0.25 mm, and the nose radius is 0.8 mm achieved the lowest cutting force of 798 N, a 15.8% reduction from the experimental average. This research replaces traditional trial-and-error approaches with systematic optimization, providing manufacturers with specific guidelines for enhancing chip control, surface quality, and tool life in industrial applications.

## ARTICLE INFO

## Article History:

Received 27 Feb 2025 Revised 11 Mar 2025 Accepted 25 Mar 2025 Available online 14 Apr 2025

#### Keywords:

Chip breaker geometry, Cutting force optimization, Finite element analysis, Taguchi method, Tool design.

### 1. INTRODUCTION

Metal cutting remains one of the fundamental manufacturing processes across engineering industries (Cascón et al., 2019; Kim et al., 2009). In today's hyper competitive manufacturing environment,

producing high-quality components at minimal cost has become essential for survival. Since raw materials often constitute 40-65% of finished product costs (depending on the sector), optimizing material utilization through improved processes delivers substantial economic

benefits (Ye et al., 2021). A critical challenge facing metalworking industries is simultaneously boosting productivity while maintaining or enhancing the quality of machined components, which demands comprehensive monitoring of machining aspects (Buchkremer et al., 2016; Devotta, 2020; Pacella, 2019). Surface roughness evaluation is not merely important but also critical across numerous engineering applications, as product lifespan attributes correlate directly with surface quality (Gurbuz et al., 2011; Shamoto et al., 2011; Shinozuka et al., 1996).

The chip formation dynamics significantly affect process efficiency and product quality when the metal is cut. As chips form, they typically curl and collide against workpieces or tools, ultimately breaking. The patterns and dimensions of these fragmented chips vary considerably, depending on the complex deformation mechanisms and collision locations. Continuous chip curling behavior follows predictable patterns: chip breakability improves when both up-curling and downcurling radii of chip clearance decrease (Yılmaz & Kıyak, 2020). Adequate external force application to the chip is essential for effective chip control. This force simultaneously decreases the chip radius while increasing the fracture strain.

Chip breakers are grooves or obstacles positioned strategically on a tool's rake face that are not just helpful. They are revolutionary for enhancing breakability. Beyond chip management, properly designed breakers reduce cutting resistance while extending tool life and workpiece improving surface characteristics through controlled chip formation (Cascón et al., 2019). Despite their importance, many machinists still select chip breakers based on gut feeling rather than science.

Finite Element (FE) modeling approaches have transformed machining process analysis by revealing detailed insights into material strain, strain rate deformation, and heat generation within primary and secondary deformation zones. FE models enable comprehensive investigation of cutting parameters' influence on chip morphology (Cascón et al., 2019; Devotta, 2020; Yılmaz & Kıyak, 2020). Predicting transitions continuous to segmented chip formations particularly important, as these transitions dramatically affect the temperatures and generated cutting forces. Segmented chips enhance breakage capability and facilitate superior process control (Cascón et al., 2019), groove-type breaker especially with designs (Yılmaz & Kıyak, 2020).

The surface properties, especially roughness parameters, critically affect the functional performance of the chip breaker. An enhanced understanding of surface generation mechanisms enables the optimization of machining processes and improves component functional capabilities (Kim et al., 2009). Numerous investigations have examined parameters including feed rate, tool nose radius, cutting speed, and depth of cut influence surface roughness during hard turning operations (Gurbuz et al., 2011; Shamoto et al., 2011; Yılmaz & Kıyak, 2020). A consistent finding shows that surface roughness decreases with increased nose radius, with larger nose radius tools producing superior surface finishes compared to smaller nose radius alternatives (Kim et al., 2009). Literature reviews have consistently identified feed rate and depth of cut as the factors that most significantly influence effective chip control and morphology.

Continuous machining processes, particularly the turning of ductile metals, frequently produce continuous chips,

which create significant handling and disposal challenges (Cascón et al., 2019; Kim et al., 2009; Ye et al., 2021). These problems intensify when machining ductile yet strong metals, such as steels, at high cutting velocities for enhanced material removal rates using flat rake face carbide or ceramic inserts. The resulting sharpedged, high-temperature continuous chips ejected at extreme velocities present serious safety hazards to operators and personnel nearby (Pacella, 2019). Additional complications include chip disposal difficulties and potential workpiece surface damage from chips entangling with rotating components. Despite the importance of chip breaker remain design, current approaches primarily based on designer experience following trial-and-error methodologies, reflecting a limited understanding of chip formation mechanisms and difficulties in predicting chip behavior from breaker designs (Shamoto et al., 2011; Yılmaz & 2020). Effective chip control necessitates accurate predictability of the chip form and breakability characteristics based on specific input machining conditions and tool geometries.

Chip formation patterns are directly correlated with manufacturing productivity. Incorrect chip formation results in multiple losses, such as operator safety hazards, damage to production equipment and workpiece surfaces, and reduced productivity from frequent Consequently, machine stoppages. breaking continuous chips into small regular fragments is essential personnel safety, product damage prevention, and efficient chip collection and disposal. Beyond these benefits, proper chip-breaking techniques enhance machinability by reducing the chip-tool contact area, lowering cutting forces, and minimizing cutting tool crater wear.

This research focuses on utilizing finite element analysis to systematically examine the influence of chip breaker geometries on cutting forces in machining processes. This study also integrates finite element analysis with the Taguchi optimization method to systematically examine six key parameters such as insert rake angle  $(\alpha)$ , insert land (a), insert radius (R), insert width (W), insert height (H), and nose radius (r) on cutting forces. Statistical validation through ANOVA and S/N ratio analysis ensured reliable findings, while the optimized chip breaker geometry demonstrated a better result in reducing cutting force. Furthermore, it incorporates an advanced material modeling approach that better captures tool-chip interactions and improves the accuracy of force predictions. Moreover, this study provides enhanced insights into chip segmentation and stress distribution, contributing to a more efficient and predictive approach to chip breaker design. This study aims to provide manufacturers with evidencebased guidance for optimizing chip breaker designs that enhance process efficiency and product quality by establishing relationships between specific geometric features and cutting performance.

# 2. RESEARCH METHODOLOGY

### 2.1. Finite Element Simulation Setup

In this study, DEFORM-3D was employed for finite element analysis to examine the cutting tool structures made from carbide and cermet materials. The approach offers significant advantages over physical testing, particularly in machining complex operations (Buchkremer et al., 2016; Devotta, 2020). DEFORM-3D slashes development costs, materials, conserves and minimizes physical testing while achieving optimal cutting conditions (Cascón et al., 2019; Pacella, 2019). The software enables a comprehensive analysis of various machining parameters and their effects on cutting performance, allowing us to conduct more reliable and efficient investigations (Buchkremer et al., 2016).

For this work, a Lagrangian-based formulation with adaptive meshing was implemented to track chip formation accurately. We applied structured mesh refinement in high-strain regions near the tool tip to improve numerical accuracy maintaining computational efficiency. The minimum element size was set at 0.04 mm for the tool and 0.075 mm for the workpiece, ensuring a sufficient resolution for capturing stress temperature gradients (Wu et 2020)We utilized the Johnson-Cook constitutive model to define the behavior of AISI 1045 carbon steel by incorporating strain hardening, strain rate sensitivity, and thermal softening effects. tungsten carbide cutting insert was treated rigid to reduce computational complexity.

Our boundary conditions involved fixing the workpiece in all degrees of freedom while assigning the tool a constant cutting speed (275 mm/min) and feed rate (0.2 mm/rev) to replicate actual machining conditions. Following the literature recommendations, a shear friction model with a coefficient of 0.6 was applied to the tool-chip interface (Wu et al., 2020). The software's extensive analysis capabilities allowed detailed examination of stress distributions, strain rates, temperature fields, and cutting forces of parameters that would be extremely challenging to measure during actual machining (Cascón et al., 2019; Devotta, 2020). Recent studies by Buchkremer et al. (Buchkremer et al., 2016) and Devotta (Devotta, 2020) have demonstrated that properly configured FEM simulations can accurately predict chip morphology and breaking behavior.

# 2.2. Workpiece and Tool Material Properties

In this study, the workpiece was modeled as a cylindrical structure with a diameter of 120 mm and a length of 200 mm. AISI 1045 carbon steel, which is commonly used in machining operations, was selected as the workpiece material (Pacella, 2019; Ye et al., 2021). The cutting insert was modeled using tungsten carbide with а diamond-shaped geometry, representing the standard industry practice for turning operations (Kim et al., 2009; Shinozuka et al., 1996). Table 1 presents the mechanical properties of the workpiece and cutting insert materials applied in the simulation. All the material property data were sourced from the DEFORM material library to ensure consistency and reliability.

Table 1: Mechanical Properties of the workpiece and cutting insert

Properties	Workpiece	Cutting insert
Materials	AISI 1045	Tungsten
		Carbide
Density (kg m <sup>-3</sup> )	7.85 x 10 <sup>-9</sup>	1.57 x 10 <sup>-8</sup>
Poisson Ratio	0.3	0.25
Elastic Module		650000
(MPa)		
Yield Strength	420	
(MPa)		
Ultimate Tensile	640	
Strength (MPa)		
% Elongation	14	
Specific Heat (J		15
kg <sup>-1</sup> K <sup>-1</sup> )		
Thermal		59
Conductivity (W		
m <sup>-1</sup> K <sup>-1</sup> )		

# 2.3. Tool Geometry and Process Parameters

The cutting tool designs incorporate various chip breaker configurations by systematically varying six key geometric parameters: insert rake angle ( $\alpha$ ), insert land (a), insert radius (R), insert width (W), insert height (H), and nose radius (r). **Figure 1** illustrates the geometric design of

the insert, while **Figure 2** shows the implementation of the 3D model in DEFORM. Recent investigations by Yilmaz and Kiyak (Yılmaz & Kıyak, 2020) and Gurbuz et al. (Gurbuz et al., 2011) have identified these parameters as particularly influential for chip control and breaking behavior.

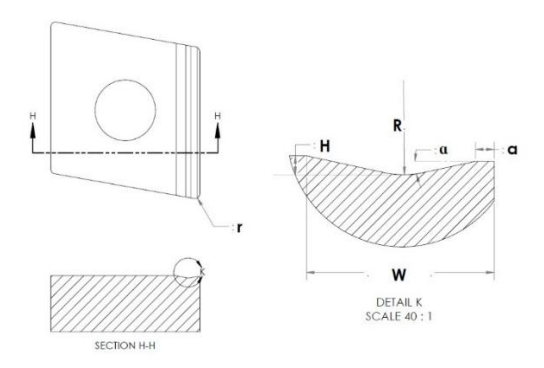


Figure 1. Illustration of the cutting insert geometry and chip breaker parameters

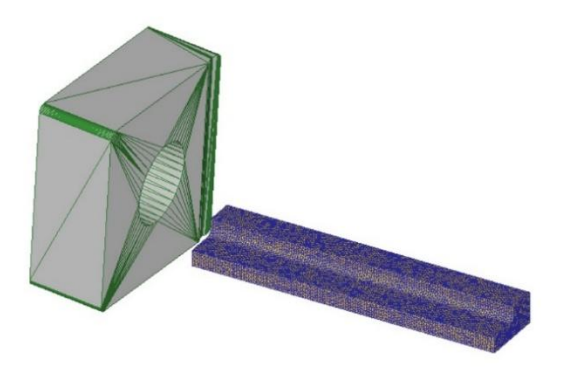


Figure 2. 3D model of the cutting insert and workpiece setup in DEFORM-3D simulation

The machining parameters (cutting speed, feed rate, and depth of cut) were maintained constant throughout all simulations to isolate the effects of tool geometry changes (Yılmaz & Kıyak, 2020). **Table 2** summarizes this study's machining parameters and tool design geometry variables. Parameter ranges were selected based on standard industrial practices and previous research findings by Hong-Gyoo et al. (Kim et al., 2009) and Cascon et al. (Cascón et al., 2019).

Table 2: Machining parameters applied to simulation

Parameter	Value		
Cutting Speed, mm/min	275		
Feed Rate, mm/rev	0.2		
Depth of Cut, mm	1.0		
Workpiece Diameter,	120		
mm			
Workpiece Length, mm	200		
Insert Rake Angle, (a)°	12	14	16
Insert Land, (a) mm	0.1	0.2	0.25
Insert Radius, (R) mm	0.5	1.0	2.0
Insert Width, (W) mm	1.5	2.0	2.5
Insert Height, (H) mm	0.2	0.25	0.4
Nose Radius, (r) mm	0.4	0.6	8.0

Table 3: Taguchi test matrix L27 orthogonal array

No.	Factor					
	Α	В	С	D	E	F
1	12	0.1	0.5	1.5	0.2	0.4
2	12	0.1	0.5	1.5	0.25	0.6
3	12	0.1	0.5	1.5	0.4	0.8
4	12	0.2	1	2.0	0.2	0.4
5	12	0.2	1	2.0	0.25	0.6
6	12	0.2	1	2.0	0.4	0.8
7	12	0.25	2	2.5	0.2	0.4
8	12	0.25	2	2.5	0.25	0.6
9	12	0.25	2	2.5	0.4	8.0
10	14	0.1	1	2.5	0.2	0.6
11	14	0.1	1	2.5	0.25	8.0
12	14	0.1	1	2.5	0.4	0.4
13	14	0.2	2	1.5	0.2	0.6
14	14	0.2	2	1.5	0.25	8.0
15	14	0.2	2	1.5	0.4	0.4
16	14	0.25	0.5	2.0	0.2	0.6
17	14	0.25	0.5	2.0	0.25	8.0
18	14	0.25	0.5	2.0	0.4	0.4
19	16	0.1	2	2.0	0.2	8.0
20	16	0.1	2	2.0	0.25	0.4
21	16	0.1	2	2.0	0.4	0.6
22	16	0.2	0.5	2.5	0.2	8.0
23	16	0.2	0.5	2.5	0.25	0.4
24	16	0.2	0.5	2.5	0.4	0.6
25	16	0.25	1	1.5	0.2	8.0
26	16	0.25	1	1.5	0.25	0.4
27	16	0.25	1	1.5	0.4	0.6

The Taguchi method was implemented to systematically evaluate each tool design parameter's relative contributions to cutting performance [9]. This approach efficiently identifies optimal parameters while minimizing the number of required simulations (Kim et al., 2009; Ye et al., 2021). **Table 3** presents the

Taguchi L27 orthogonal array test matrix utilized in the finite element analysis to identify the configurations that produce lower cutting forces. In the Taguchi test, insert rake angle, insert land, insert radius, insert width, insert height and nose radius are represented by Factor A, B, C, D, E, and F, respectively.

# 2.4. Experimental Design using the Taguchi Method

The L27 orthogonal array was selected as the most suitable experimental design for investigating three levels of six factors (insert rake angle, land, radius, width, height, and nose radius). This array requires minimum tests to investigate the tool design parameters comprehensively (Shinozuka et al., 1996; Yılmaz & Kıyak, 2020). The experimental design and subsequent analysis were developed using MINITAB statistical software.

# 2.5. Signal-to-Noise Ratio Analysis

Signal-to-noise ratio (S/N Ratio) analysis was conducted to determine the optimal parameter settings for minimizing cutting force. The S/N ratio represents the relationship between the desired value (signal) and undesired effects (noise) during experimentation (Pacella, 2019; Shamoto et al., 2011). In this study, cutting force was designated as the desired response variable. At the same time, the effects of the insert rake angle, land, radius, width, height, and nose radius were considered as noise factors.

Three categories of S/N ratio are commonly employed in Taguchi analysis: "nominal is better," "smaller is better," and "larger is better" (Gurbuz et al., 2011; Ye et al., 2021). For this investigation, the "smaller is better" approach was selected for the cutting force response, as lower cutting forces generally indicate better

machining performance (Shinozuka et al., 1996). The S/N ratio was calculated using Equation 1, where yi represents the response value for the ith test and n is the total number of tests.

$$\frac{s}{N} = -10\log\left[\frac{1}{n}\sum_{i=1}^{n}y_i^2\right] \quad (1)$$

## 3. RESULTS AND DISCUSSION

## 3.1 Main Effects Analysis

The influence of the six geometric parameters (A-F) on cutting force was systematically analyzed using the Taguchi method. **Table 4** presents the average main effect values for cutting force obtained from each factor (A: insert rake angle, B: insert land, C: insert radius, D: insert width, E: insert height, and F: nose radius) at each level (1, 2, and 3). These values represent the mean response for each factor level across all experiments.

**Figure 3** illustrates the main effects plot for the cutting force, graphically representing the data from **Table 4**. The quality characteristic used in this analysis was "smaller is better" for cutting force, as lower cutting forces are generally preferable in machining operations to reduce power consumption, tool wear, and thermal effects.

Table 4: Average main effect results for cutting force

Level		Factor					
	Α	В	С	D	E	F	
1	969.2	931.9	929.1	969.6	927.9	1002.4	
2	945.8	954.8	949.1	911.5	927.3	930.2	
3	914.1	942.4	948.7	944.4	973.9	896.4	
Delta	55.1	22.9	20.0	58.1	46.6	106.0	
Rank	3	5	6	2	4	1	

From the main effects analysis, it is evident that the optimal parameter combination for minimizing cutting force is A3B1C1D2E2F3, corresponding to an insert rake angle of 16° (A3), an insert land of 0.1 mm (B1), an insert radius of 0.5 mm (C1), an insert width of 2.0 mm (D2), an insert

height of 0.25 mm (E2), and a nose radius of 0.8 mm (F3).

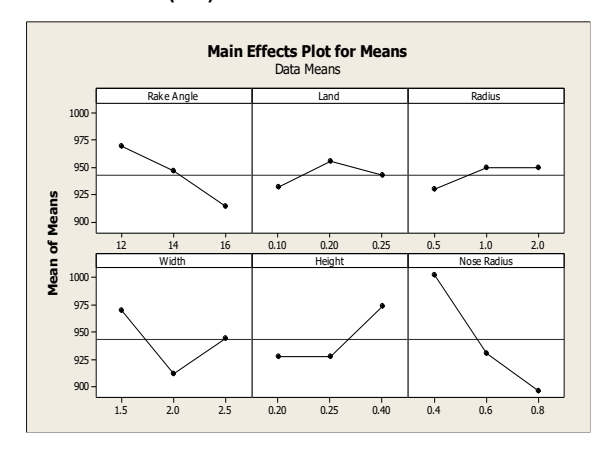


Figure 3: Main effects plots for means

The slope of each factor's line in the main effects plot indicates the magnitude of its influence on cutting force. Factor F (nose radius) shows the steepest slope, confirming its dominant effect on cutting force, followed by factors D (insert width) and A (rake angle). The lowest point on its respective curve identifies the optimal level for each factor, as lower cutting force values are desirable.

# 3.2. Signal-to-Noise Ratio Analysis

Signal-to-Noise (S/N) ratio analysis was performed to determine the robustness of the parameter settings against noise factors. Using Equation 1, the S/N ratio was calculated for each experimental run, with results in **Table 5**. For the "smaller is better" characteristic, higher (less negative) S/N ratio values indicate more desirable performance.

The highest S/N ratio value of -58.2018 dB was observed in experiment 19, indicating the most favorable condition for minimizing cutting force. This observation aligns with the measured cutting force value of 813 N in this simulation, representing one of the lowest cutting forces recorded in the study. The S/N ratio analysis confirms that the optimal parameter settings identified in the main

effects analysis are robust against variations in the process.

Table 5: Results of S/N ratio analysis

No.	f Smaller is be	Smaller is better						
experimen	t							
	Force (N)	S/N Ratio (dB)						
1	1040	-60.3407						
2	952	-59.5727						
3	947	-59.5270						
4	1010	-60.0864						
5	883	-58.9192						
6	986	-59.8775						
7	967	-59.7085						
8	968	-59.7175						
9	970	-59.7354						
10	927	-59.3416						
11	868	-58.7704						
12	989	-59.9039						
13	976	-59.7890						
14	903	-59.1138						
15	1090	-60.7485						
16	893	-59.0170						
17	856	-58.6495						
18	1010	-60.0864						
19	813	-58.2018						
20	943	-59.4902						
21	908	-59.1617						
22	847	58.5577						
23	990	59.9127						
24	908	59.1617						
25	878	58.8699						
26	983	59.8511						
27	957	59.6182						

# 3.3. Analysis of Variance (ANOVA)

Analysis of Variance (ANOVA) was conducted to statistically evaluate the significance of each geometric parameter on cutting force. **Table 6** presents the ANOVA results obtained from MINITAB software.

The ANOVA results reveal that factor F (nose radius) significantly influences cutting force, with an F-ratio of 27.41 and a P-value of 0.000, indicating statistical significance at a 99% confidence level. This is followed by factor A (rake angle) with an F-ratio of 7.66 (P-value: 0.006), factor E (insert height) with an F-ratio of 6.34 (P-value: 0.011), and factor D (insert width) with an F-ratio of 5.77 (P-value: 0.015).

Factors B (insert land) and C (insert radius) show relatively minor influences on cutting force, with F-ratios of 1.35 and 0.31, respectively, and P-values exceeding 0.05, indicating these parameters are not statistically significant at the 95% confidence level.

Table 6: ANOVA for cutting force

Sourc	D	Seq	Adj	MS	F	Р
е	F					
Α	2	13769.	13694.	6847.2	7.66	0.00
		0	3			6
В	2	2362.3	2404.4	1202.2	1.35	0.29
						2
С	2	2174.6	559.1	279.5	0.31	0.73
						6
D	2	15500.	10319.	5159.9	5.77	0.01
		4	8			5
E	2	9726.1	11339.	5669.9	6.34	0.01
			8			1
F	2	48979.	48979.	24489.	27.4	0.00
		9	9	9	1	0
Error	1	12510.	12510.	893.6		
	4	7	7			
Total	2	15371				
	6	4				

S = 29.8935 R-Sq = 88.09% R-Sq(adj) = 77.88%

The R-squared value of 88.09% indicates that 88.09% of the variation in cutting force can be explained by the six geometric parameters examined in this study, demonstrating a strong relationship between the tool geometry and resulting cutting forces. The adjusted R-squared value of 77.88% accounts for the number of predictors in the model and still indicates a good fit.

# 3.4. Optimization and Verification

Based on the main effects analysis and ANOVA results, the Taguchi method suggested an optimal parameter combination of A3B1C1D2E2F3, corresponding to insert rake angle of 16°, insert land of 0.1 mm, insert radius of 0.5 mm, insert width of 2.0 mm, insert height of 0.25 mm, and nose radius of 0.8 mm. A verification simulation was conducted using these optimal parameters to validate the prediction.

The verification simulation resulted in a cutting force of 798 N, which represents significant improvement over the average 947.7 N across all 27 experimental optimized configuration runs. This achieved a 15.8% reduction in cutting force compared to the experimental average and a 26.8% reduction compared to the highest cutting force value of 1090 N observed in experiment 15. In comparison, Vasumathy et al. (2017) achieved only a 5% reduction in cutting force, demonstrating that the optimization approach in this study provides a significantly greater improvement in machining efficiency.

Figure 4 displays the strain and stress distributions obtained from the simulation using the optimized tool geometry. The strain distribution (left) shows the localized deformation in the primary and secondary shear zones, while the stress distribution (right) illustrates the concentration of stresses at the tool-chip interface. The optimized geometry promotes chip segmentation, facilitating chip breaking and reducing cutting forces.

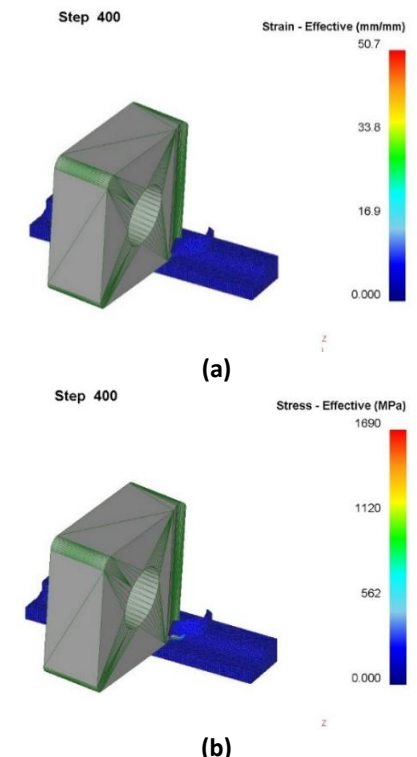


Figure 4(a). Strain and (b) stress result for optimum tool design

The stress distribution reveals that the maximum stress occurs at the tool-chip interface near the cutting edge. However, the optimized tool geometry effectively distributes this stress over a larger area, potentially reducing tool wear. The strain distribution shows effective chip segmentation, essential for proper chip breaking. These results confirm that the optimized tool geometry reduces cutting force and promotes favorable chip formation characteristics.

### 3.5. Discussion of Parameter Effects

The significant influence of nose radius (factor F) on cutting force can be attributed to its direct impact on the contact area between the tool and the workpiece. A larger nose radius of 0.8 mm (level 3) distributes the cutting force over a larger area, reducing the localized stress and force required for material removal. This finding aligns with previous studies, such as those by Yilmaz and Kiyak (2020), who reported that a larger nose radius improves cutting force characteristics and surface finish. Similarly, Zhang et al. (2024) examined how varying nose radii affected tool wear and chip formation in GH3536 nickel-based superalloys. Their results showed that a larger nose radius increased tool wear due to work hardening. In contrast, the 0.8 mm nose radius in this study effectively reduced cutting force (798 N) without a notable negative impact on tool life.

The insert rake angle (factor A) showed the second most significant effect on cutting force. The optimal level of 16° (level 3) provides a more inclined surface for chip flow, reducing friction and the energy required for chip formation. This confirms the established machining principle that higher rake angles (within practical limits) reduce cutting forces by facilitating easier chip flow. A similar trend was observed in Zhang et al. (2024), where

their 04VP3 chip breaker (15° rake angle, flat-bottom groove) improved chip breakability over their 04HA design (9° rake angle, V-bottom groove). Their study reinforces the importance of rake angle optimization in enhancing chip segmentation and controlling cutting forces, supporting the effectiveness of the 16° rake angle chosen in this study.

Insert width (factor D) and insert height (factor E) also significantly affected cutting force, with optimal levels of 2.0 mm and 0.25 mm, respectively. These dimensions influence the chip flow path and breaking mechanism, affecting how efficiently the chip is formed and evacuated from the cutting zone. The findings align with Wu et al. (2020), who demonstrated that chip breaker groove design significantly affects chip segmentation and force distribution in AISI 1045 carbon steel. The relatively minor influence of insert land (factor B) and insert radius (factor C) suggests that while these parameters contribute to overall chip breaker performance, they are less critical for force reduction than the nose radius, rake angle, and chip breaker width.

## 4. CONCLUSION

This study investigated the effects of six geometric parameters (insert rake angle, insert land, insert radius, insert width, insert height, and nose radius) on cutting forces during turning operations using finite element analysis. Based on the comprehensive analysis of the simulation results, the nose radius emerged as the most significant factor influencing cutting force, with an F-ratio of 27.41 in the **ANOVA** analysis. This parameter's substantial impact can be attributed to its direct effect on the tool-chip contact area and resulting stress distribution during machining. The rake angle and insert width were identified as the second and third

most influential parameters, with F-ratios of 7.66 and 5.77, respectively. These parameters significantly affect chip flow and the resulting dynamics requirements during cutting (Zhang et al., 2024). Using the Taguchi method, an optimal tool geometry configuration was established with the following parameters: insert rake angle of 16°, insert land of 0.1 mm, insert radius of 0.5 mm, insert width of 2.0 mm, insert height of 0.25 mm, and nose radius of 0.8 mm. The optimized tool geometry achieved a cutting force of 798 N, representing a significant reduction to non-optimized compared configurations. This reduction in cutting force demonstrates the potential for improved tool life, reduced power consumption, and enhanced machining efficiency. Strain and stress analysis of the optimized configuration revealed effective chip segmentation patterns, indicating improved chip breaking capability. This characteristic is particularly valuable for industrial applications where chip control is critical for process stability and safety. The findings from this research provide valuable insights for cutting manufacturers and machining process planners, offering evidence-based guidelines for chip breaker design optimization. Significant improvements in cutting performance can be achieved by strategically configuring these geometric parameters, particularly focusing on nose radius optimization.

## **REFERENCES**

- Buchkremer, S., Klocke, F., & Veselovac, D. (2016). 3D FEM simulation of chip breakage in metal cutting. *The International Journal of Advanced Manufacturing Technology*, *82*(1), 645–661. https://doi.org/10.1007/s00170-015-7383-9
- Cascón, I., Sarasua, & Elkaseer, A. (2019). Tailored Chip Breaker Development for Polycrystalline Diamond Inserts: FEM-Based Design and Validation. *Applied Sciences*, *9*, 4117. https://doi.org/10.3390/app9194117
- Devotta, A. M. (2020). *Improved finite element modelingfor chip morphology prediction inmachining of C45E steel*. University West.
- Gurbuz, H., Kurt, A., Çiftçi, İ., & Şeker, U. (2011). The Influence of Chip Breaker Geometry on Tool Stresses in Turning. *Strojniski Vestnik*, *57*, 91–99. https://doi.org/10.5545/sv-jme.2009.191
- Kim, H.-G., Sim, J.-H., & Kweon, H. J. (2009). Performance evaluation of chip breaker utilizing neural network. *Journal of Materials Processing Technology*, 209, 647–656. https://api.semanticscholar.org/CorpusID:108955911
- Pacella, M. (2019). A new low-feed chip breaking tool and its effect on chip morphology. *The International Journal of Advanced Manufacturing Technology*, 104. https://doi.org/10.1007/s00170-019-03961-2
- Shamoto, E., Aoki, T., Sencer, B., Suzuki, N., Hino, R., & Koide, T. (2011). Control of chip flow with guide grooves for continuous chip disposal and chip-pulling turning. *CIRP Annals*, 60(1), 125–128. https://doi.org/https://doi.org/10.1016/j.cirp.2011.03.081
- Shinozuka, J., Obikawa, T., & Shirakashi, T. (1996). Chip breaking analysis from the viewpoint of the optimum cutting tool geometry design. *Journal of Materials Processing*

- *Technology*, *62*(4), 345–351. https://doi.org/https://doi.org/10.1016/S0924-0136(96)02433-8
- Wu, L., Liu, J., Ren, Y., Yang, Z., Wang, G., Sun, J., Song, J., Xu, W., & Liu, X. (2020). 3D FEM simulation of chip breakage in turning AISI1045 with complicate-grooved insert. *The International Journal of Advanced Manufacturing Technology*, 108(5), 1331–1341. https://doi.org/10.1007/s00170-020-05460-1
- Ye, Z., Lv, D., & Wang, Y. (2021). Design of chip breaker and study on cutting performance in reaming 7050 aluminum alloy. *The International Journal of Advanced Manufacturing Technology*, 116, 1–15. https://doi.org/10.1007/s00170-021-07393-9
- Yılmaz, Y., & Kıyak, M. (2020). Investigation of Chip Breaker and Its Effect in Turning Operations. *Journal of Advances in Manufacturing Engineering*, 1(1), 29–37. https://dergipark.org.tr/en/pub/jame/issue/65465/1011877
- Zhang, X., Li, M., Soo, S., & Yang, X. (2024). Effects of chip breaker groove and tool nose radius on progressive tool wear and behavior when turning GH3536 nickel-based superalloys. *Tribology International*, 197, 109806. https://doi.org/10.1016/j.triboint.2024.109806